2023

Design and Implementation Of A New Adaptive MPPT Controller For Solar PV Systems

Saibal Manna

Deepak Kumar Singh

Ashok Kumar Akella

See next page for additional authors

Funder: European Union's Horizon 2020 Research and Enterprise Ireland under the Marie Skłodowska-Curie Grant 847402.

Authors

Saibal Manna, Deepak Kumar Singh, Ashok Kumar Akella, Hossam Kotb, Kareem M. AboRas, Hossam Zawbaa, and Salah Kamel

Energy Reports 9 (2023) 1818–1829

Contents lists available at ScienceDirect

Energy Reports

journal homepage: www.elsevier.com/locate/egyr

Research paper

Design and implementation of a new adaptive MPPT controller for solar PV systems

Saibal Manna [a,*], Deepak Kumar Singh [a], Ashok Kumar Akella [a], Hossam Kotb [b], Kareem M. AboRas [b], Hossam M. Zawbaa [c,d,e,**], Salah Kamel [f]

[a] Department of Electrical Engineering, NIT Jamshedpur, Jharkhand, India
[b] Department of Electrical Power and Machines, Faculty of Engineering, Alexandria University, Alexandria, Egypt
[c] Faculty of Computers and Artificial Intelligence, Beni-Suef University, Beni-Suef, Egypt
[d] Technological University Dublin, Dublin, Ireland
[e] Applied Science Research Center, Applied Science Private University, Amman, Jordan
[f] Electrical Engineering Department, Faculty of Engineering, Aswan University, 81542 Aswan, Egypt

ARTICLE INFO

Article history:
Received 30 August 2022
Received in revised form 22 November 2022
Accepted 31 December 2022
Available online 5 January 2023

Keywords:
Solar photovoltaic
Model reference adaptive control
MIT rule
Maximum power point tracking
Boost converter

ABSTRACT

This research provides an adaptive control design in a photovoltaic system (PV) for maximum power point tracking (MPPT). In the PV system, MPPT strategies are used to deliver the maximum available power to the load under solar radiation and atmospheric temperature changes. This article presents a new adaptive control framework to enhance the performance of MPPT, which will minimize the complexity in system control and efficiently manage uncertainties and disruptions in the environment and PV system. Here, the MPPT algorithm is decoupled with model reference adaptive control (MRAC) techniques, and the system gains MPPT with overall system stability. The simulation and design of the new MRAC for MPPT based on a boost converter are addressed here. Moreover, a mathematical model is formulated and an efficient MRAC is designed for MPPT. To validate the robustness of the controller, MATLAB/Simulink is utilized to compare with the state-of-the-art approach, which is incremental conductance (INC) and perturb & observe (P&O) under various operating conditions based on the convergence time, tracking efficiency, PV current & voltage ripple, overall efficiency, and error rates. The proposed controller's average tracking efficiency is 99.77% and 99.69% under diverse temperature and radiation conditions, respectively. In addition, it takes only 3.6 msec to capture MPP, which is around ten times faster than INC and twelve times faster than the P&O approach. When compared to INC and P&O, the MPP error rates in the MRAC-MPPT scheme are significantly lower. The simulation outcomes indicate that the presented controller exhibits excellent tracking under varying circumstances like solar radiation and temperature.

1. Introduction

The demand for renewable energy is growing, lowering prices and offering a future for clean energy. This clean energy revolution is powered by solar and wind energy. It is understood that the energy generated by the sun is safe and available for free on earth 24 h a day. Solar systems are supplying 1.7 percent of the worldwide demand for electricity, and by 2025 the production capacity should exceed 1 TW (Singh et al., 2022). In comparison to electricity generation by fossil fuels, solar-generated electricity does not cause greenhouse gas emissions (A low amount of greenhouse gas can emit during panel manufacturing and after-life recycling practices, but less than fossil fuel resources). Furthermore, solar energy is a secure energy source, particularly in countries with little or no fossil fuel supplies. Basically, in all PV systems — PV panels, DC/AC converter, charge controller, and batteries are four important components that make it simple to set up in both homes and commercial premises.

Atmospheric conditions, dust, temperature, cloud cover, and geographical location are the primary factors that reduce the amount of solar energy that may be harvested. The intensity of solar radiation naturally changes in the daytime due to the changing hourly azimuth angle of the radiation. Even on a gloomy day, the sunshine is lower than the sun on a bright day. The amount of electricity produced from any PV panel differs depending on the panel's resistive load, which decreases the generation

* Corresponding author.
** Corresponding author at: Technological University Dublin, Dublin, Ireland.
E-mail addresses: mannasaibal1994@gmail.com (S. Manna), dksingh1946@gmail.com (D.K. Singh), akakella.ee@nitjsr.ac.in (A.K. Akella), hossam.kotb@alexu.edu.eg (H. Kotb), kareem.aboras@alexu.edu.eg (K.M. AboRas), hossam.zawbaa@gmail.com (H.M. Zawbaa), skamel@aswu.edu.eg (S. Kamel).

https://doi.org/10.1016/j.egyr.2022.12.152

of electricity even with the same irradiance and temperatures. At a given load value, the maximum power point (MPP) exists and varies during the day with temperature and irradiance fluctuations, making it challenging to find and calculate the MPP (Li et al., 2020; Bollipo et al., 2020). The manuscript's main focus is on MPPT, not other PV obstacles. The key MPPT topologies used for solar cells to monitor the MPP include buck-boost, boost, and buck converters. The boost converter's low switching losses and low inductivity, which minimizes current ripples, make it ideal for PV applications. Also, this converter has a steady current with lower current stress compared to other topologies during converter operation (Podder et al., 2019).

In order to optimize their performance, MPPT devices need a control algorithm. The proportional–integral–derivative (PID) controller is commonly utilized in MPPT systems due to its simplicity and flexibility in implementation. However, PID demonstrates a low performance for MPPT applications with its simple structure (Kler et al., 2018). Traditional methods, such as INC (Jagadeshwar and Das, 2022), and P&O (Manna et al., 2022a), are the most widely utilized. Conventional approaches, despite their simple structure and application, were only capable of tracking the MPP while the weather remained constant. Furthermore, traditional MPPT algorithms exhibit oscillations near the MPP and are ineffective for large-scale solar power facilities. Due to the aforementioned restrictions, engineers and researchers throughout the globe are developing novel methods for controlling MPPT in solar systems.

Soft computing, artificial intelligence (AI), and bio-inspired (BI) are some of the most important advanced MPPT technologies that can alleviate some of the issues raised by standard MPPT controllers (Li et al., 2022). In spite of their complexity, advanced MPPT techniques have a great ability to track the MPP. Heuristic approaches like genetic algorithm (GA) (Mirza et al., 2020), particle swarm optimization (PSO) (Renaudineau et al., 2015), fuzzy logic control (FLC) (Pan et al., 2020), and artificial neural network(ANN) (Tavakoli and Forouzanfar, 2020a) are some of the most common advanced MPPT techniques. The MPPT methodology based on soft computing is among the most powerful ways of solving nonlinear problems. Unfortunately, these MPPT algorithms are more complex, need a precise training dataset, and are more expensive to deploy than classic methods.

The literature is rich with studies aiming to improve upon current methods and address their shortcomings. A novel fuzzy logic (FL) based hybrid MPPT approach is proposed for solar systems. An offline short circuit current is used to determine the MPP approximatively, and the FL approach is then used to determine the accurate value of maximum power. The proposed approach was simulated in the MATLAB/Simulink environment. The outcomes showed that the proposed method outperformed the hybrid approach (open-circuit voltage and P&O approach) in a variety of environmental settings (Parvaneh and Khorasani, 2020). A novel P&O approach is implemented, which is optimized via neural network (NN) technology for the purpose of MPPT. Simulation tests were conducted to verify the system's functionality under varying levels of solar radiation. The proposed research reveals that when using different light intensities and temperatures, the NN-optimized P&O approach outperforms the traditional INC approaches. This controller is shown to be capable of producing about 99% of the true maximum power. In contrast to INC, which takes about 0.3 s to reach the reference value, the NN approach takes just about 0.025 s, with minimum overshoot (Saidi et al., 2021). A rapid and optimal approach for MPPT has been developed using FL without the assistance of a trained expert to create membership functions. MATLAB is used to carry out the methodology and assess its effectiveness. According to the results, the FL is far superior to the ANN-PSO, ANN-GA, and ANN-ICA (imperialist competitive algorithm) with respect to stability, accuracy, speed, and ease of implementation against environmental fluctuations (Fathi and Parian, 2021). To alleviate the chattering issue, a super-twisting sliding mode controller was designed, and a type 2 fuzzy set (STSMC-T2FC) was implemented into the system. The proposed algorithm is designed in MATLAB and compared with STSMC & traditional SMC under varying radiation conditions. The STSMC-T2FC MPPT has an efficiency of 99.59%, whereas STSMC achieves 99.33% and SMC achieves 99.20%. Even though the efficiency performances are close, STSMC-T2FC came out on top (Kayisli, 2023). A robust direct adaptive controller (RDAC) based on a boost converter is designed for MPPT. The controller's reliability under different operation conditions is verified by MATLAB/Simulink once a mathematical model has been built, and a suitable RDAC is designed for the MPPT (Bani Salim et al., 2019). A two-stage global MPPT control mechanism was suggested to ensure that all of the power produced by the PV is sent to load. The first stage is global perturbation-based extremum seeking control (GPESC) and is used to locate global MPP. The second stage is MRAC, which is used to manage the DC–DC converter dynamics. The simulation tests the proposed controller performance with respect to tracking speed, efficiency, and accuracy across a range of radiation conditions. Here, the GPESE and GPESC-PID controllers are used for comparison (Dadkhah Tehrani and Shabaninia, 2018). To quickly reach MPP in response to changes in radiation and temperature, a new approach is created using the modified MRAC in conjunction with the Lyapunov and INC approach. To illustrate the robustness of control law, simulations using PSIM will be presented to show how the proposed controller tracks the MPP in comparison to the INC-PI controller (Tariba et al., 2016). An MPPT controller for the PV system that uses an adaptive neuro-fuzzy inference system (ANFIS) is provided under changing environmental conditions. When compared to P&O and FLC, the proposed approach can track the MPP more quickly in variable weather circumstances (Haji and Naci, 2020). An improved MPPT method based on FLC has been developed. The proposed approach has an accuracy of 99.5% to 99.9% under a wide variety of radiation and temperature conditions. Even more impressive is the fact that MPP can be recorded in just 21 ms, which is four and five times faster than P&O and INC, respectively. Additionally, the proposed technique was compared to the traditional FLC, and it was shown that the suggested method is 28% faster and has a 1% higher efficiency than the FLC method (Yilmaz et al., 2019).

As per the brief literature survey, traditional approaches are easy to implement and produce good results for MPPT but suffer from the drawback of experiencing undesirable oscillations close to MPP. On the other hand, soft-computing methods are the most powerful for tracking MPPT, but they are complex, expensive, and require huge computational time. Hence, this has motivated the author to develop an adaptive controller that can alleviate the drawbacks of conventional and soft-computing approaches. Therefore, it is a real challenge to make a thorough improvement to the performance of the MPPT algorithm with respect to complexity, tracking speed, accuracy, oscillations near MPP, and tracking efficiency under changing environmental conditions. In literature, the traditional MRAC is designed for a first-order system. However, the majority of plants, including PV systems with boost converters, are second-order systems. Traditional MRAC tracking performance for second-order systems is unsatisfactory. This article presents the new MRAC framework extended from the first order to the second order to enhance MPPT's performance, which will minimize complexity in system control and efficiently manage the uncertainties and disruptions in the environment and PV system. The novelty of the proposed research is to derive MRAC control law for second

order PV MPPT system. The proposed technique features simple, higher dynamic response, negligible oscillations near MPP, fast tracking speed, and higher efficiency under dynamic weather conditions. The MATLAB/Simulink software is utilized for the proposed controller's design, simulation, and benchmarking. The proposed controller's average tracking efficiency is 99.77% and 99.69% under diverse temperature and radiation conditions, respectively. In addition, the average convergence time is 3.6 ms to capture MPP under dynamic environmental conditions. The output indicates that the controller exhibits excellent tracking under varying circumstances like solar radiation and temperature changes. The following is a summary of the proposed research's primary contribution:

- A new MRAC controller is proposed for solar PV systems for efficient MPPT.
- The proposed controller features simple implementation, higher dynamic response, fast convergence time, high efficiency, and negligible oscillations near MPP.
- Being adaptive, MRAC is robust to radiation and temperature change.
- The proposed controller obtained results are vividly compared with most popular classical algorithms like INC and P&O with respect to convergence time, current ripple, voltage ripple, tracking efficiency, overall efficiency, root mean square error (RMSE), mean absolute error (MAE) and mean absolute percentage error (MAPE).
- It has a convergence speed that is ten and twelve times as fast as that of the INC and P&O approaches, respectively.

This paper is divided into four major parts: The mathematical model of the PV system is discussed in Section 2. Section 3 discusses the dynamics of boost converters and how they can be integrated into PV systems. Section 4 details the steps taken during the MRAC design process. Research results from the simulation are presented in Section 5. The paper's conclusion is provided in Section 6.

2. PV system model and characteristics

The most typical configuration of a PV cell consists of the components shown in Fig. 1, which are a current source, a diode, and a set of resistors connected in parallel and series. The current generated by a solar cell can be calculated using the following formulas (Manna et al., 2022b):

$$i_{pv} = I_R - I_{d1} - I_{pe} \tag{1}$$

where i_{pv} and v_{pv} denote PV array output current and voltage, respectively. I_{pe}, I_R, and I_{d1} present parallel resistance (R_{pe}), PV, and diode current. The series resistance is denoted as R_{se}.

$$I_{d1} = I_{01}\left(e^{q\frac{(v_{pv}+i_{pv}R_{se})}{nKT}} - 1\right) \tag{2}$$

where I_{01} indicates reverse saturation current. T, q, K and n symbolizes temperature, electron charge, Boltzmann constant, and diode factor, respectively.

Eq. (3) gives the fundamental expression for the current generated by a PV cell.

$$I_R = \frac{W}{W_0}(I_c + \lambda(T - T_0)) \tag{3}$$

Short circuit current is denoted by the symbol I_c. W_0 and T_0 symbolizes reference irradiance and temperature respectively. W and λ denote irradiance and temperature coefficient, respectively.

$$i_{pv} = I_R - I_{01}\left[e^{q\frac{(v_{pv}+i_{pv}R_{se})}{nKT}} - 1\right] - \frac{v_{pv} + R_{se}i_{pv}}{R_{pe}} \tag{4}$$

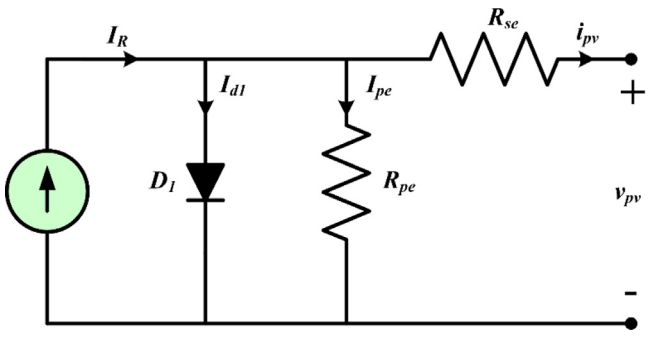

Fig. 1. Solar cell equivalent circuit.

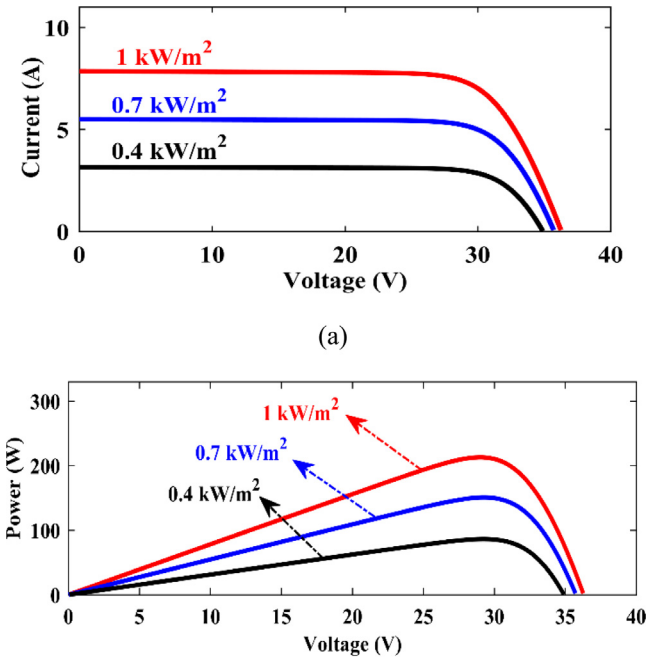

Fig. 2. (a) The current–voltage and (b) power–voltage graphs obtained at various radiation with 25 °C (Yilmaz et al., 2019).

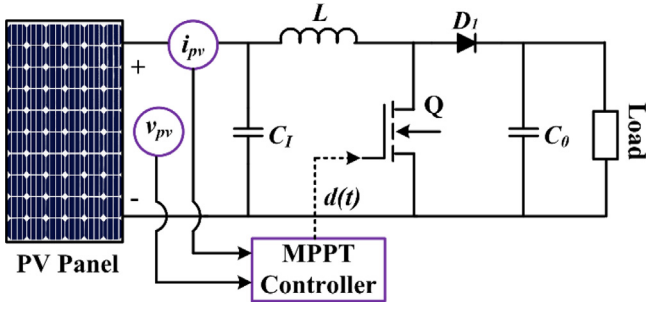

Fig. 3. PV system with MPPT controller and boost converter.

The I_{01} is defined by:

$$I_{01} = I_{01ref}\left(\frac{T}{T_0}\right)^3 e^{\left[\frac{qE_G}{nK}\left(\frac{1}{T}-\frac{1}{T_0}\right)\right]}. \tag{5}$$

where E_G is the energy bandgap.

The power generated from a single solar cell is relatively low (1–1.5 W). In order to achieve demanded power, solar cells can be

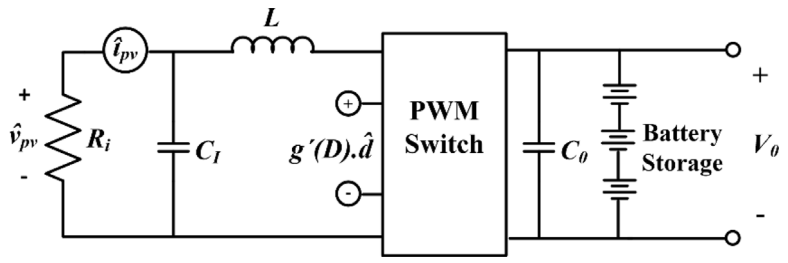

Fig. 4. PV array's small signal equivalent circuit to boost converter (Khanna et al., 2014).

connected into series to produce panels and panels, either in parallel or series, in order to create photovoltaic arrays. To be more specific, as shown in Fig. 2, the MPP varies with environmental circumstances, necessitating the use of a controller to adjust the PV load in a manner that is as close as possible to the MPP.

As shown in Fig. 2(b), the MPP holds true when there is no change in power as a function of voltage. The equation that captures this relationship looks like Eq. (6)

$$\frac{dp}{dv_{pv}} = \begin{cases} = 0, \textit{ at MPP} \\ > 0, \textit{ at left side of MPP} \\ < 0, \textit{ at right side of MPP} \end{cases} \tag{6}$$

This equation will serve as the control rule for the MPPT adaptive controller.

3. Boost converter model

Fig. 3 shows the boost converter that is used to provide maximum power to the load, demonstrating its usefulness in modern systems. Other converters can be utilized instead of this converter, depending on the application. Fig. 4 depicts the boost converter approach, in which the MPPT controller monitors the solar array's voltage and current levels and feeds the duty cycle ($d(t)$) to the switch Q. Eq. (7) links the $d(t)$ to the voltage of the array.

$$v_{pv} = i_{pv} R_0 (1-d)^2 \tag{7}$$

where the current and voltage of the PV array are indicated by i_{pv} and v_{pv}. The load resistance is denoted as R_0. Ripple ($\hat{v}_{pv}$ and $\hat{\imath}_{pv}$) and DC (V_{PV} and I_{PV}) components are present in the voltage and current of a PV array. Next, a controller that continuously monitors the loop's optimal value must be developed to guarantee that V_{PV} follows V_M and I_{PV} follows I_M in order to generate the highest possible power.

The conventional MPPT approach to calculating the steady-state duty cycle relies on the basis provided by Eq. (7). The MPPT control should consider the relationship between the duty cycle and the array voltage to maximize the transient response. After adjusting the duty cycle for varying environmental circumstances, MPPT controllers must suppress oscillations from the array voltage because transitory oscillations are undesired and can add to device inefficiency. In Messo et al. (2012), a detailed dynamic model of the boost converter is presented and discussed. In order to make the study of transient response more understandable, it is believed that the system can be represented by a small-signal equivalent circuit, as discussed in Femia et al. (2005). The PV small-signal equivalent circuit is shown in Fig. 4. Resistor R_i, small-signal array voltage ($\hat{v}_{pv}$), and current ($\hat{\imath}_{pv}$) across its terminal are used to represent the solar array.

At this point, the transfer function (TF) is determined between the control signal ($d(t)$) and the voltage across the array at a given operating point. The dynamics of the system are presented in this TF. Fig. 4 illustrates a dynamic model with a battery load typical of a PV system. Here, the TF between the duty cycle and the array voltage is derived under small signal operation, ignoring the battery dynamics in the process. From this analysis of Fig. 4, we obtain the following correlation (Khanna et al., 2014).

$$\frac{\hat{v}_{pv}(s)}{R_i} + s\hat{v}_{pv}(s) C_I = \frac{g'(D)\,\hat{d}(s) - \hat{v}_{pv}(s)}{sL} \tag{8}$$

where $\hat{d}(s)$ symbolized small-signal variation around the converter's duty cycle D. The connection between V_{PV} and D is denoted by $g(D)$. The derivative of $g(D)$ with respect to D is written as $g'(D)$. Based on Eq. (8), we obtain:

$$\frac{\hat{v}_{pv}(s)}{\hat{d}(s)} = \frac{g'(D)}{LC_I s^2 + \frac{L}{R_i} s + 1} \tag{9}$$

It is well known that

$$g(D) = V_{PV} = (1-D)\,V_0 \tag{10}$$

The steady-state output of the boost converter is denoted as V_0. Assuming that $g(D)$ and V_0 are not affected by transient switching behavior leads to the Eq. (10). From (10), $g'(D) = -V_0$ and now Eq. (9) will be

$$\frac{\hat{v}_{pv}(s)}{\hat{d}(s)} = \frac{-\frac{V_0}{LC_I}}{s^2 + \frac{L}{R_i C_I} s + \frac{1}{LC_I}} \tag{11}$$

The negative indication shows that an increase in panel voltage occurs when the duty ratio is decreased. Parasitic power-stage components were excluded from this analysis. The aforementioned TF is determined for a nonlinear system (shown in Fig. 3) near a single operating point using the linearized version (shown in Fig. 4).

4. Proposed adaptive controller design

This section presents the MRAC design, which is intended to maximize the power generated by a PV system. The general schematic architecture of recommended control strategy is shown in Fig. 5. The MPPT control law is denoted by Eq. (6), and the controller's reference voltage is adjustable in accordance with Eq. (12), where Δv is the small threshold voltage. As displayed in Fig. 6, the v_{ref} calculation block of the suggested MPPT approach is depicted as a flowchart.

$$v_{ref} = \begin{cases} v_{pv}, \dfrac{dp}{dv_{pv}} = 0. \\ v_{pv} - \Delta v, \dfrac{dp}{dv_{pv}} < 0. \\ v_{pv} + \Delta v, \dfrac{dp}{dv_{pv}} > 0. \end{cases} \tag{12}$$

Due to its adaptability, adaptive control technology can handle unexpected events, modifications, and disturbances in the system's structure, as well as alterations to the operational conditions. MRAC was developed for MPP applications because of its unique properties and simplicity of implementation.

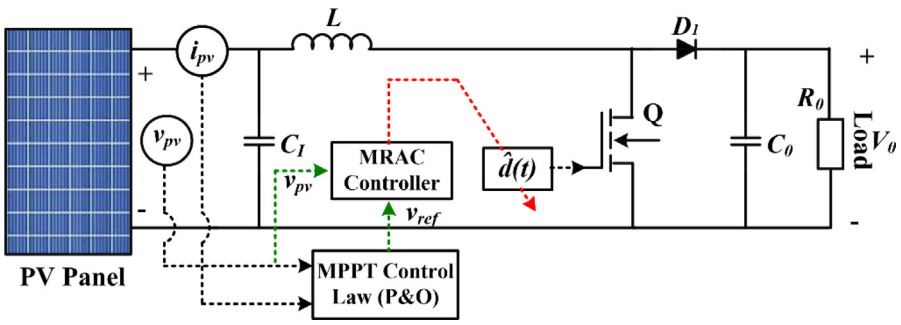

Fig. 5. MPPT adaptive controller for PV system.

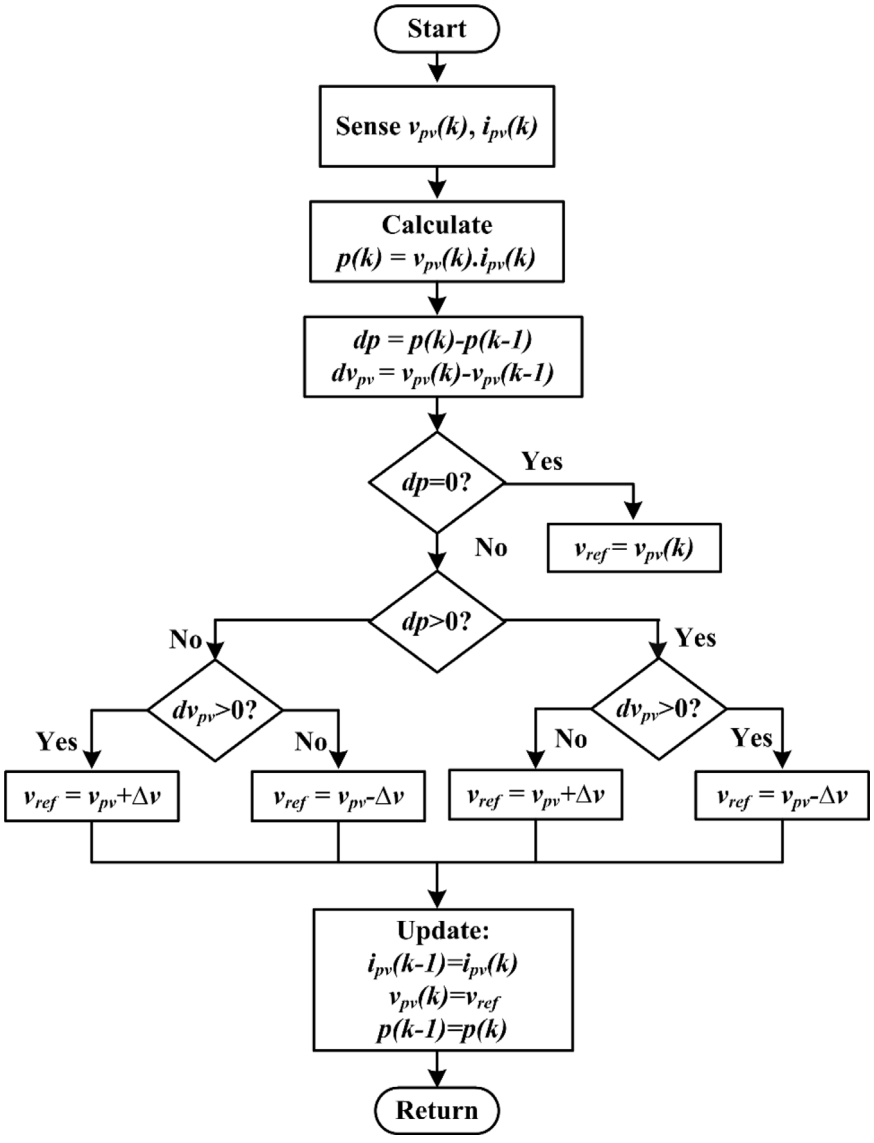

Fig. 6. Reference voltage flowchart.

The only two inputs that MRAC needs are the array and reference voltages. The reference model, plant, and adaptation gain (γ) make up the backbone of the MRAC.

The goal of MRAC is to have the primary plant output mimic the output of the reference model through the use of γ. When developing an MRAC, it is necessary to select a reference model to represent the best possible output response, and then create a controller to reduce the error (e) between the reference and the actual plant output. Among the most fundamental adaptive approaches, the MIT law is one that uses a gradient strategy. The MRAC controller, pioneered at MIT in the 1960s for use in aerospace applications, takes this technique by modifying the adaptation laws in order to minimize the e difference between the reference and system output. In literature, the traditional MRAC is designed for a first-order system. However, the majority of plants, including PV systems with boost converters, are

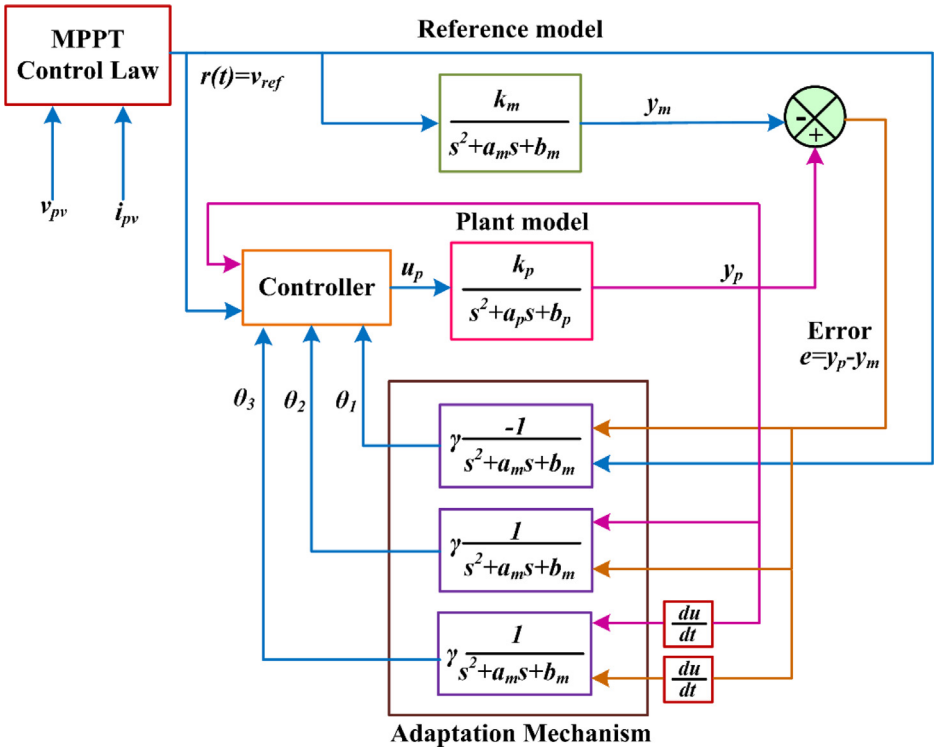

Fig. 7. New MRAC controller architecture.

second-order systems. Traditional MRAC tracking performance for second-order systems is unsatisfactory. The control law for the second order system along with extension from the first to the second order of MRAC is derived here. Fig. 7 illustrates the proposed controller structure.

The second-order plant model is selected (time and frequency domain) with the following form

$$\frac{d^2y_p(t)}{dt^2} = -a_p\frac{dy_p(t)}{dt} - b_p y_p(t) + k_p u_p(t) \tag{13}$$

$$G_p(s) = \frac{y_p(s)}{u_p(s)} = \frac{k_p}{s^2 + a_p s + b_p} \tag{14}$$

where a_p, b_p, and k_p is the plant parameter and can be calculated from Eq. (11).

The second-order reference model has been selected (time and frequency domain) to show the desired output $y_m(t)$ for input $r(t)$ with the following form

$$\frac{d^2y_m(t)}{dt^2} = -a_m\frac{dy_m(t)}{dt} - b_m y_m(t) + k_m r(t) \tag{15}$$

$$G_m(s) = \frac{y_m(s)}{r(s)} = \frac{k_m}{s^2 + a_m s + b_m} \tag{16}$$

where k_m is a positive gain, a_m, and b_m are calculated so that the reference model generates a critically damped step response. The control strategy's purpose is to build $u_p(t)$ in such a way that $y_p(t)$ asymptotically follows $y_m(t)$.

The MIT rule is used to construct the adaptation law for the controller parameters in MRAC. By applying the MIT rule, the cost function is written as follows:

$$J(\theta) = \frac{e^2}{2} \tag{17}$$

$$e = y_p - y_m \tag{18}$$

The error (e) here is the difference between the plant model (y_p) and the reference model (y_m). The adjustable control parameter is denoted as θ. The control parameter θ is modified in accordance with the MIT rule in order to minimize the value of the cost function as indicated by Eq. (17). Thus, we can write:

$$\frac{d\theta}{dt} = -\gamma\frac{\delta J}{\delta\theta} = -\gamma e\frac{\delta e}{\delta\theta} \tag{19}$$

where $\frac{\delta e}{\delta\theta}$ & γ are defined as sensitivity derivative and adaptation gain, respectively. The controller structure is depicted in Fig. 7 to achieve the desired control objectives. For bounded reference input, the control law u_p is considered to be

$$u_p = \theta_1 r - \theta_2 y_p - \theta_3\dot{y}_p = \theta^T\varphi \tag{20}$$

where φ is defined as $\left[r, y_p, \dot{y}_p\right]^T$ and $[\theta_1, \theta_2, \theta_3]^T$ is the controller parameter estimation vector.

Substituting Eq. (20) into Eq. (13), we get

$$\frac{d^2y_p(t)}{dt^2} = -\left(a_p + k_p\theta_3\right)\frac{dy_p(t)}{dt} - \left(b_p + k_p\theta_2\right)y_p(t) + k_p\theta_1 r(t) \tag{21}$$

Comparing Eqs. (15) and (21) coefficient, we get

$$k_p\theta_1 = k_m \tag{22}$$

$$b_m = b_p + k_p\theta_2 \tag{23}$$

$$a_m = a_p + k_p\theta_3 \tag{24}$$

where θ_1, θ_2, and θ_3 are control parameters are converged as:

$$\theta_1 \approx \frac{k_m}{k_p};\quad \theta_2 \approx \frac{b_m - b_p}{k_p};\quad \theta_3 \approx \frac{a_m - a_p}{k_p} \tag{25}$$

Taking Laplace to transform in Eq. (21), we get

$$\frac{y_p(s)}{r(s)} = \frac{k_p\theta_1}{s^2 + \left(a_p + k_p\theta_3\right)s + \left(b_p + k_p\theta_2\right)} \tag{26}$$

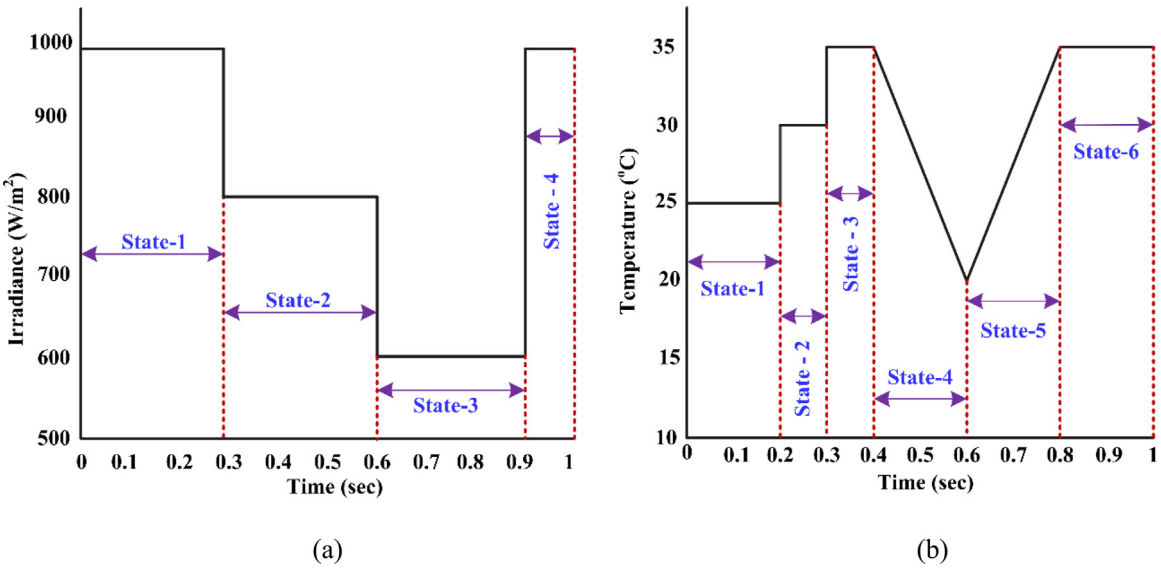

Fig. 8. (a) Solar radiation variation (b) Temperature variation signal profile.

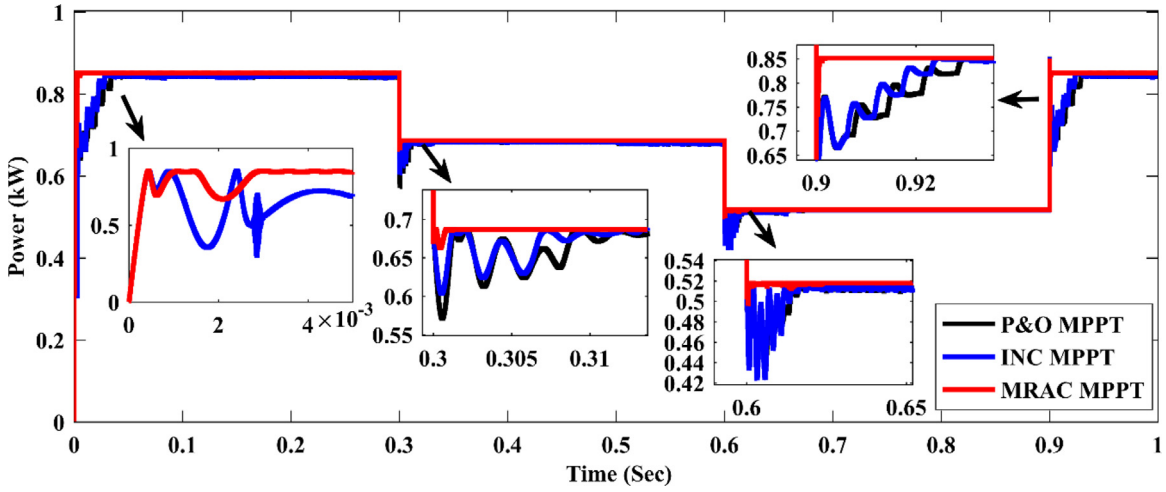

Fig. 9. The PV power utilizing three MPPT strategies under variable irradiance and constant temperature.

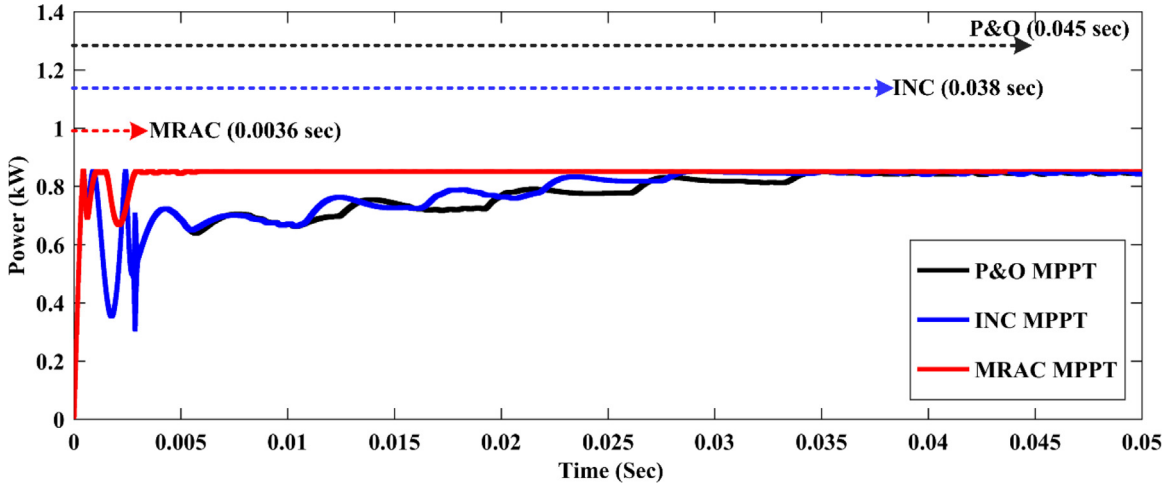

Fig. 10. The MPPT approaches speed with varying irradiance and constant temperature.

Table 1
Simulation parameters.

Parameter	Value	Parameter	Value
Rated power (P_{MPP})	213.15 W	Boost inductor (L)	2 mH
Rated current (I_{MPP})	7.35 A	Load value (R_0)	20 Ω
Short-circuit current (I_{sc})	7.84 A	Boost output capacitor (C_0)	100 μF
Rated voltage (V_{MPP})	29 V	Output voltage range (V_0)	112.5–129.1 V
Open-circuit voltage (V_{oc})	36.3 V	$a_p = 1/R_i \times C_I$	400 (rad/s)
Number of parallel modules	2	a_m	8.17×10^3 (rad/s)
PV cell R_{pe}	313.3991 Ω	$b_p = 1/L \times C_I$	1.67×10^7 (rad/s)^2
Number of series module	2	b_m	1.67×10^7 (rad/s)^2
PV cell R_{se}	0.39383 Ω	$K_p = V_0/L \times C_I$	6.45×10^8 V (rad/s)^2
Cells per module	60	k_m	5.75×10^8 V (rad/s)^2
R_i	25 Ω	Adaptation gain (γ)	0.08
Boost input capacitor (C_I)	100 μF	Switching frequency (f_s)	20 kHz
Input voltage range (V_{IN})	56.6-60.3 V	Simulation step time (T_s)	1 μs

Table 2
Detail comparison of three algorithms with 4 states.

MPPT techniques	State 1	State 2	State 3	State 4
Voltage ripple (V)				
P&O	4.03	3.07	4.88	3.63
INC	3.97	2.93	4.06	3.36
MRAC	0.04	0.01	0.02	0.03
Current ripple (A)				
P&O	0.96	0.57	0.62	0.94
INC	1.10	0.55	0.60	0.92
MRAC	0.034	0.22	0.004	0.045
Convergence time (s)				
P&O	0.045	0.032	0.042	0.043
INC	0.038	0.026	0.038	0.035
MRAC	0.0036	0.0052	0.004	0.0038
Tracking efficiency (%)				
P&O	97.90	97.50	97.93	97.90
INC	98.10	97.90	98.05	98.10
MRAC	99.94	99.20	99.67	99.94
Overall efficiency (%)				
P&O	95.08	96.11	97.65	95.38
INC	95.39	96.81	97.95	95.50
MRAC	98.54	98.08	98.69	98.57
Error rate at finding MPP, RMSE error				
P&O	0.00545	0.00388	0.00635	0.00537
INC	0.00540	0.00381	0.00640	0.00536
MRAC	0.00053	0.00054	0.00067	0.00052
MAE error				
P&O	0.00451	0.00352	0.00681	0.00446
INC	0.00450	0.00351	0.00638	0.00441
MRAC	0.00052	0.00054	0.00067	0.00052
MAPE error (%)				
P&O	0.528	0.517	1.249	0.526
INC	0.510	0.513	1.239	0.524
MRAC	0.061	0.080	0.013	0.061

As per error Eq. (18), we can write

$$e = \left(\frac{k_p \theta_1}{s^2 + \left(a_p + k_p \theta_3\right) s + \left(b_p + k_p \theta_2\right)} - \frac{k_m}{s^2 + a_m s + b_m} \right) r(s) \tag{27}$$

The sensitivity derivatives $\frac{\delta e}{\delta \theta_1}$, $\frac{\delta e}{\delta \theta_2}$ and $\frac{\delta e}{\delta \theta_3}$ are derived from Eqs. (27) and (26) given by

$$\frac{\delta e}{\delta \theta_1} = \frac{k_p r}{s^2 + a_p s + k_p \theta_3 s + b_p + k_p \theta_2} \tag{28}$$

$$\frac{\delta e}{\delta \theta_2} = \frac{-k_p y_p}{s^2 + a_p s + k_p \theta_3 s + b_p + k_p \theta_2} \tag{29}$$

$$\frac{\delta e}{\delta \theta_3} = \frac{-k_p y_p s}{s^2 + a_p s + k_p \theta_3 s + b_p + k_p \theta_2} \tag{30}$$

Considering $s^2 + a_m s + b_m = s^2 + a_p s + k_p \theta_3 s + b_p + k_p \theta_2$. As per the MIT rule (Eqs. (17) and (19)), the sensitivity derivatives are substituted in Eq. (19). After rearranging, the Eqs. (31), (32), and (33) are used to update the control parameters θ_1, θ_2, and θ_3, respectively.

$$\frac{d\theta_1(t)}{dt} = -\gamma \left(\frac{1}{s^2 + a_m s + b_m} r(t) \right) e(t) \tag{31}$$

$$\frac{d\theta_2(t)}{dt} = \gamma \left(\frac{1}{s^2 + a_m s + b_m} y_p(t) \right) e(t) \tag{32}$$

$$\frac{d\theta_2(t)}{dt} = \gamma \left(\frac{1}{s^2 + a_m s + b_m} \dot{y}_p(t) \right) \dot{e}(t) \tag{33}$$

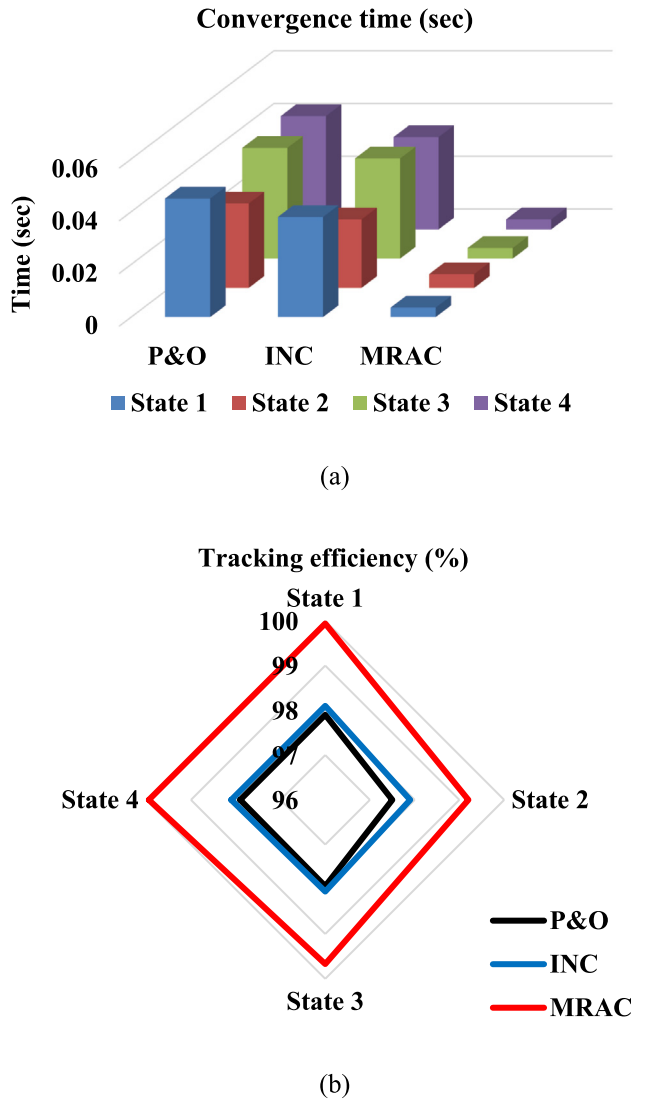

Fig. 11. Comparison evaluation (a) Convergence time (b) Tracking efficiency.

Now MRAC controller design is completed in this section, and the results are reported in the next section.

5. Simulation results and discussion

The Simulink toolbox was used to simulate the MRAC-based MPPT. The simulation is made up of three key interrelated parts: adaptive controller, PV, and boost converter. Table 1 lists all the user-defined simulation parameters for the proposed system. Under rapidly changing temperature and radiation, detailed comparisons of the new controller are done with state-of-the-art techniques like P&O and INC. The tracking efficiency (η) of the algorithms is calculated as (Tavakoli and Forouzanfar, 2020b)

$$\eta = \frac{\int_{t_1}^{t_2} P_{avg}\,dt}{\int_{t_1}^{t_2} P_{max}\,dt} \tag{34}$$

The algorithm begins its tracking at time t_1, and ends at time t_2. In this context, P_{avg} refers to the average power achieved between t_1 & t_2 time period and P_{max} is the theoretically available maximum power. The voltage and current ripple refer to the peak-to-peak value of voltage and current respectively.

5.1. Under rapidly changing solar radiation with constant temperature

Fig. 8(a) shows the radiation signal variation. The chosen signals have four states. Throughout this process, the temperature has been at a steady 25 °C. Fig. 9 depicts the PV power using three different MPPT algorithms (Proposed MPPT, INC, and P&O) under rapidly fluctuating solar radiation conditions. The relative speed of different MPPT methods is shown in Fig. 10.

It can be shown in Fig. 10 that the P&O method has a maximum lag time of 0.045 s to adopt MPP, followed by the INC technique at 0.038 s, while the proposed technique only takes 0.0036 s to capture MPP. The INC and P&O methods have ripple content close to MPP but fail to achieve MPP, whereas MRAC has practically zero ripple content and easily tracks MPP over all four irradiation stages. While analyzing the convergence time the values are 0.045 s, 0.032 s, 0.042 s, and 0.043 s in states 1 to 4 respectively for the P&O scheme. In the case of the INC scheme convergence times are 0.038 s, 0.026 s, 0.038 s, and 0.035 s in states 1 to 4 respectively. While considering the new technique, the time to follow MPP is very fast and the values are 0.0036 s, 0.0052 s, 0.004 s, and 0.0038 s in states 1 to 4, respectively. The tracking efficiency of the P&O technique is between 97.90%–97.93%; for the INC technique, it is between 97.90%–98.10%, whereas for the proposed technique, it is between 99.20% to 99.94%.

The maximum value of RMSE, MAE, and MAPE is 0.00635, 0.00681, and 1.249%, respectively for P&O, 0.00640, 0.00638, and 1.239%, respectively in the case of INC, and 0.00067, 0.00067, 0.080% respectively in the case of the proposed technique. Table 2 shows the detailed comparison of three algorithms with respect to current ripple, convergence time, voltage ripple, tracking efficiency, overall efficiency, and error in four states. Fig. 11 shows the graphical representation of convergence time and tracking efficiency for all three MPPT techniques. So, it can be concluded that the voltage and current ripple are minimum, convergence times are minimum, tracking efficiency is higher, overall efficiency is higher, and error rates are lowest in the case of the suggested MPPT controller. Thus, the new controller provides the best performance among the other two MPPT techniques under rapidly varying radiation conditions.

5.2. Under rapidly changing temperatures with constant radiation

Fig. 8(b) shows the varying temperature signal, considering a total of six states in this signal. During this procedure, the radiation is held steady at 1000 W/m^2. The simulated comparison of the maximum PV power that may be generated utilizing the MRAC, P&O, and INC MPPT techniques is shown in Fig. 12. Fig. 13 shows that although the P&O method requires a maximum of 0.049 s, the INC method requires 0.042 s, and the proposed method requires just 0.0038 s to follow MPP. In contrast to MRAC's practically zero ripple content and straightforward MPP tracking over all six irradiation stages, P&O and INC's methods have ripple content close to MPP but fail to achieve MPP. Table 3 shows the detailed comparison of three algorithms with respect to current ripple, convergence time, tracking efficiency, voltage ripple, overall efficiency, and error in six states.

So, it can be concluded that the voltage and current ripple are minimum, convergence times are minimum, tracking efficiency is higher, overall efficiency is higher, and error rates are lowest in the case of the MRAC-MPPT controller under changing radiation and temperature circumstances. Thus, the proposed controller provides the best performance among the other two MPPT techniques under rapidly varying radiation and temperature conditions. Table 4 provides an in-depth comprehensive analysis of the most up-to-date MPPT techniques with the proposed MPPT approach.

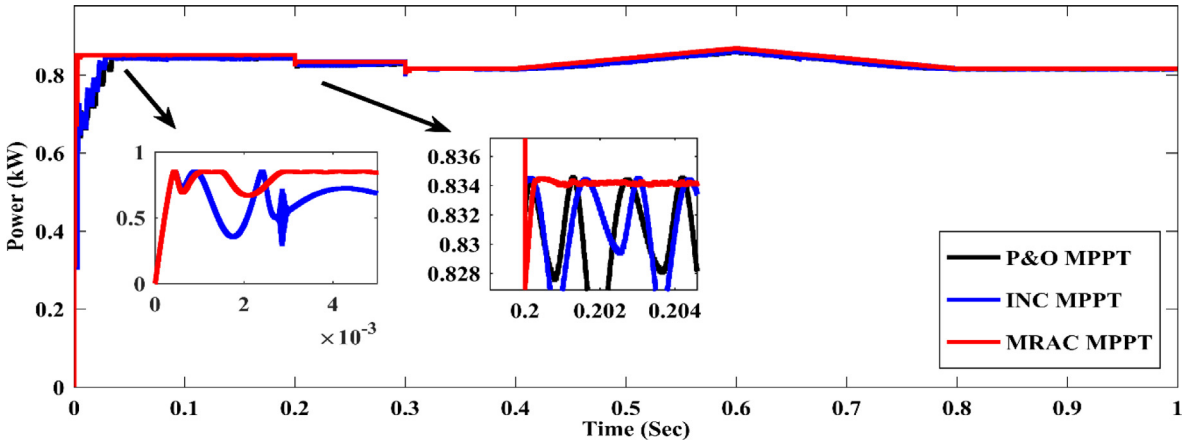

Fig. 12. The PV power utilizing three MPPT strategies under variable temperature and constant irradiance.

Table 3
Detail comparison of three algorithms with six states.

MPPT techniques	State 1	State 2	State 3	State 4	State 5	State 6
Voltage ripple (V)						
P&O	4.07	3.88	1.49	4.10	4.82	1.43
INC	3.63	3.78	1.46	3.57	4.66	1.40
MRAC	0.08	0.04	0.01	0.01	0.02	0.05
Current ripple (A)						
P&O	1.11	1.15	0.48	1.03	0.1	0.43
INC	1.06	1.06	0.44	0.97	0.98	0.42
MRAC	0.04	0.03	0.046	0.03	0.02	0.021
Convergence time (s)						
P&O	0.049	0.041	0.042	0.041	0.043	0.040
INC	0.042	0.035	0.035	0.036	0.036	0.032
MRAC	0.0038	0.005	0.0039	0.0056	0.004	0.0032
Tracking efficiency (%)						
P&O	97.47	97.32	95.52	97.93	96.10	95.01
INC	97.48	97.46	95.81	98.20	96.89	95.71
MRAC	99.94	99.90	99.85	99.65	99.46	99.85
Overall efficiency (%)						
P&O	95.38	93.39	91.73	95.92	92.26	91.73
INC	96.01	94.39	92.68	96.92	93.62	93.77
MRAC	98.84	98.82	98.78	98.19	98.43	98.78
Error rate at finding MPP, RMSE error						
P&O	0.00541	0.02272	0.03675	0.01391	0.04398	0.03874
INC	0.00530	0.02182	0.03569	0.01287	0.03400	0.03568
MRAC	0.00052	0.00178	0.00353	0.00145	0.00332	0.00353
MAE error						
P&O	0.00550	0.03150	0.04574	0.01273	0.03398	0.03573
INC	0.00451	0.02159	0.03568	0.01269	0.03396	0.03568
MRAC	0.00052	0.00178	0.00353	0.00145	0.00332	0.00353
MAPE error (%)						
P&O	0.5289	2.824	4.195	1.494	3.994	4.194
INC	0.5100	2.534	4.188	1.489	3.986	4.187
MRAC	0.0617	0.209	0.415	0.170	0.389	0.415

6. Conclusion

Adaptive control techniques found widespread application in time-varying or nonlinear systems due to their capacity to respond to unexpected changes in inputs or system dynamics. Additionally, adaptive controllers frequently require less prior knowledge of the system and less computational time. This article incorporates the use of the model reference adaptive controller to set the PV output voltage to the MPP under rapidly changing radiation and temperature situations. The outcomes prove that the proposed MRAC method is highly efficient. The efficiency of the innovative MPPT method ranges from 99.20% to 99.94%, while P&O and INC range from 97.90% to 97.93% and 97.90% to 98.10%, respectively. The recommended MPPT technique results in the lowest MPP oscillation rate, faster convergence time, higher efficiency, negligible ripple, and lower error rate compared to the alternatives. This propels the method to the top of the efficiency rankings. In addition, it takes only 3.6 ms to capture MPP, which is around ten times faster than INC and twelve times faster than the P&O approach. In the future, this work will focus on designing MRAC-based MPPT for partial shading conditions.

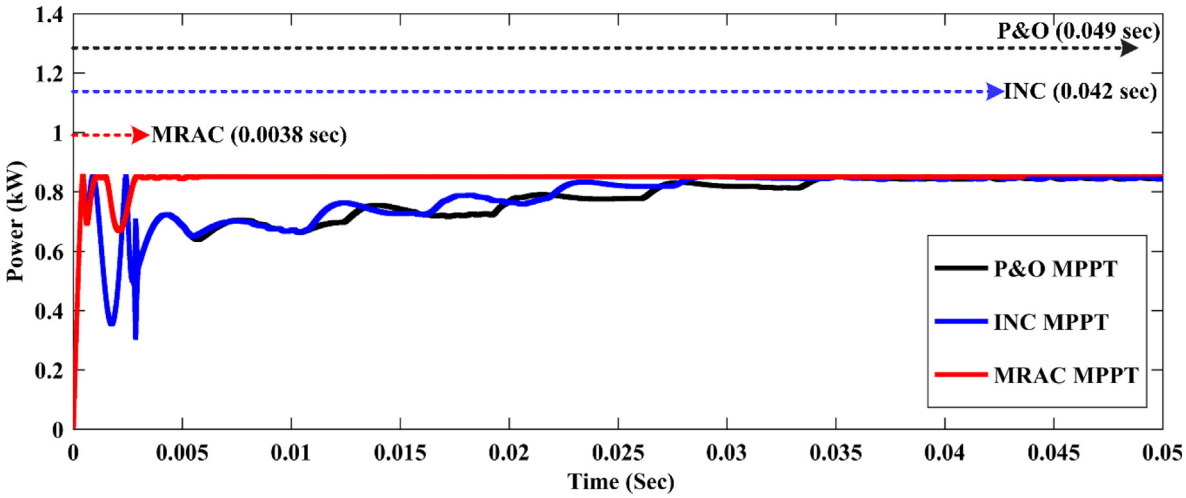

Fig. 13. The MPPT approaches speed with varying temperatures and constant irradiance.

Table 4
Comparative analysis of the proposed approach with other techniques.

Algorithm	Complexity	Convergence time (s)	Efficiency	Steady-state oscillation	Input variables (sensed)
Quantized input-SMC (Aminnejhad et al., 2021)	Medium	<1.8	98.9%	No	Voltage and current
Grey wolf optimization (GWO)-PID (Aguila-Leon et al., 2023)	Medium	0.018	99.50%	No	Voltage and current
Variable step GA-INC (Feroz Mirza et al., 2020)	Medium	0.013	99.09%	No	Voltage and current
Self-constructing Lyapunov neural network (SCLNN)-MRAC (Tavakoli and Forouzanfar, 2020b)	Medium	0.021	98.14%	Low	Voltage and current
Hybrid whale optimization and pattern search (HWO-PS)-ANFIS-INC (Tao et al., 2021)	High	0.13	99.35%	Low	Radiation, temperature, and voltage
Reduced oscillation-based P&O (Pathak et al., 2022)	Medium	0.018	99.49%	No	Voltage and current
Proposed MPPT	Low	0.0036	99.69%	No	Voltage and current

CRediT authorship contribution statement

Saibal Manna: Conceptualization, Formal analysis, Writing – review & editing. **Deepak Kumar Singh:** Conceptualization, Formal analysis, Writing – review & editing. **Ashok Kumar Akella:** Investigation, Writing – review & editing. **Hossam Kotb:** Conceptualization, Supervision, Writing – review & editing. **Kareem M. AboRas:** Conceptualization, Supervision, Writing – review & editing. **Hossam M. Zawbaa:** Funding, Writing – review & editing. **Salah Kamel:** Supervision, Writing – review & editing.

Declaration of competing interest

The authors declare that they have no known competing financial interests or personal relationships that could have appeared to influence the work reported in this paper.

Data availability

Data will be made available on request.

Acknowledgments

The work of Hossam M. Zawbaa was supported by the European Union's Horizon 2020 Research and Enterprise Ireland under the Marie Skłodowska-Curie Grant 847402.

References

Aguila-Leon, Jesus, Vargas-Salgado, Carlos, Chiñas-Palacios, Cristian, Díaz-Bello, Dácil, 2023. Solar photovoltaic Maximum Power Point Tracking controller optimization using Grey Wolf Optimizer: A performance comparison between bio-inspired and traditional algorithms. Expert Syst. Appl. (ISSN: 0957-4174) 211, 118700. http://dx.doi.org/10.1016/j.eswa.2022.118700.

Aminnejhad, Hojjat, Kazeminia, Sarang, Aliasghary, Mortaza, 2021. Robust sliding-mode control for maximum power point tracking of photovoltaic power systems with quantized input signal. Optik (ISSN: 0030-4026) 247, 167983. http://dx.doi.org/10.1016/j.ijleo.2021.167983.

Bani Salim, M., Hayajneh, H.S., Mohammed, A., Ozcelik, S., 2019. Robust direct adaptive controller design for photovoltaic maximum power point tracking application. Energies 12 (16), 3182. http://dx.doi.org/10.3390/en12163182.

Bollipo, R.B., Mikkili, S., Bonthagorla, P.K., 2020. Critical review on PV MPPT techniques: Classical, intelligent and optimisation. IET Renew. Power Gener. 14 (9), 1433–1452.

Dadkhah Tehrani, R., Shabaninia, F., 2018. Two-level control of photovoltaic systems using global perturbation-based extremum seeking control and model reference adaptive control. Trans. Inst. Meas. Control 40 (13), 3709–3720. http://dx.doi.org/10.1177/0142331217731620.

Fathi, Milad, Parian, Jafar Amiri, 2021. Intelligent MPPT for photovoltaic panels using a novel fuzzy logic and artificial neural networks based on evolutionary algorithms. Energy Rep. 7, 1338–1348. http://dx.doi.org/10.1016/j.egyr.2021.02.051.

Femia, N., Petrone, G., Spagnuolo, G., Vitelli, M., 2005. Optimization of perturb and observe maximum power point tracking method. IEEE Trans. Power Electron. 20 (4), 963–973.

Feroz Mirza, A., Mansoor, M., Ling, Q., Khan, M.I., Aldossary, O.M., 2020. Advanced variable step size incremental conductance MPPT for a standalone PV system utilizing a GA-tuned PID controller. Energies 13 (16), 4153. http://dx.doi.org/10.3390/en13164153.

Haji, D., Naci, G., 2020. Dynamic behaviour analysis of ANFIS based MPPT controller for standalone photovoltaic systems. Int. J. Renew. Energy Res. 10 (1), 101–108.

Jagadeshwar, M., Das, D.K., 2022. A novel adaptive model predictive control scheme with incremental conductance for extracting maximum power from a solar panel. Iran. J. Sci. Technol. Trans. Electr. Eng. http://dx.doi.org/10.1007/s40998-022-00495-4.

Kayisli, Korhan, 2023. Super twisting sliding mode-type 2 fuzzy MPPT control of solar PV system with parameter optimization under variable irradiance conditions. Ain Shams Eng. J. 14 (1), 101950. http://dx.doi.org/10.1016/j.asej.2022.101950.

Khanna, R., Zhang, Q., Stanchina, W.E., Reed, G.F., Mao, Z., 2014. Maximum power point tracking using model reference adaptive control. IEEE Trans. Power Electron. 29 (3), 1490–1499. http://dx.doi.org/10.1109/TPEL.2013.2263154.

Kler, Dhruv, Rana, K.P.S., Kumar, Vineet, 2018. A nonlinear PID controller based novel maximum power point tracker for PV systems. J. Franklin Inst. B 355 (16), 7827–7864.

Li, K., Liu, C., Jiang, S., Chen, Y., 2020. Review on hybrid geothermal and solar power systems. J. Clean. Prod. 250, 119481.

Li, Jianlin, Wu, Yiwen, Ma, Suliang, Chen, Mingxuan, Zhang, Baoping, Jiang, Bing, 2022. Analysis of photovoltaic array maximum power point tracking under uniform environment and partial shading condition: A review. Energy Rep. 8, 13235–13252. http://dx.doi.org/10.1016/j.egyr.2022.09.192.

Manna, S., Akella, A.K., Singh, D.K., 2022a. A novel MRAC-MPPT scheme to enhance speed and accuracy in PV systems. Iran. J Sci. Technol. Trans. Electr. Eng. http://dx.doi.org/10.1007/s40998-022-00542-0.

Manna, S., Singh, D.K., Akella, A.K., Abdelaziz, A.Y., Prasad, M., 2022b. A novel robust model reference adaptive MPPT controller for Photovoltaic systems. Sci. Iran. http://dx.doi.org/10.24200/sci.2022.59553.6312.

Messo, T., Jokipii, J., Suntio, T., 2012. Steady-state and dynamic properties of boost-power-stage converter in photovoltaic applications. In: Proc. 3rd IEEE Int. Symp. Power Electron. Distrib. Generat. Syst. (PEDG 2012), Jun.. pp. 34–40.

Mirza, A.F., Mansoor, M., Ling, Q., Khan, M.I., Aldossary, O.M., 2020. Advanced variable step size incremental conductance MPPT for a standalone PV system utilizing a GA-tuned PID controller. Energies (Basel) 13 (6), 13164153.

Pan, Z., Quynh, N.V., Ali, Z.M., Dadfar, S., Kashiwagi, T., 2020. Enhancement of maximum power point tracking technique based on PV-Battery system using hybrid BAT algorithm and fuzzy controller. J. Clean. Prod. 274, 123719.

Parvaneh, Mohammad Hasan, Khorasani, Pouria Goharshenasan, 2020. A new hybrid method based on Fuzzy Logic for maximum power point tracking of Photovoltaic Systems. Energy Rep. 6, 1619–1632. http://dx.doi.org/10.1016/j.egyr.2020.06.010.

Pathak, Pawan Kumar, Yadav, Anil Kumar, Alvi, P.A., 2022. Reduced oscillations based perturb and observe solar maximum power point tracking scheme to enhance efficacy and speed of a photovoltaic system. J. Eng. Res. http://dx.doi.org/10.36909/jer.13569.

Podder, A.K., Roy, N.K., Pota, H.R., 2019. MPPT methods for solar PV systems: a critical review based on tracking nature. IET Renew. Power Gener. 13, 1615–1632. http://dx.doi.org/10.1049/iet-rpg.2018.5946.

Renaudineau, H., Donatantonio, F., Fontchastagner, J., Petrone, G., Spagnuolo, G., Martin, J.P., Pierfederici, S., 2015. A PSO-based global MPPT technique for distributed PV power generation. IEEE Trans. Ind. Electron. 62 (2), 1047–1058.

Saidi, Abdelaziz Salah, Salah, Chokri Ben, Errachdi, Ayachi, Azeem, Mohammad Fazle, Bhutto, Javed Khan, Thafasal Ijyas, V.P., 2021. A novel approach in stand-alone photovoltaic system using MPPT controllers & NNE. Ain Shams Eng. J. 12 (2), 1973–1984. http://dx.doi.org/10.1016/j.asej.2021.01.006.

Singh, D.K., Akella, A.K., Manna, S., 2022. Deterministic and probabilistic analysis of different empirical models to estimate monthly mean diffuse solar radiation for composite climatic region of India. Environ. Prog. Sustain. Energy 41 (6), e13917. http://dx.doi.org/10.1002/ep.13917.

Tao, Hai, Ghahremani, Mehrdad, Ahmed, Faraedoon Waly, Jing, Wang, Nazir, Muhammad Shahzad, Ohshima, Kentaro, 2021. A novel MPPT controller in PV systems with hybrid whale optimization-PS algorithm based ANFIS under different conditions. Control Eng. Pract. (ISSN: 0967-0661) 112, 104809. http://dx.doi.org/10.1016/j.conengprac.2021.104809.

Tariba, N., Haddou, A., El Omari, H., El Omari, H., 2016. Design and implementation an adaptive control for MPPT systems using model reference adaptive controller. In: 2016 International Renewable and Sustainable Energy Conference. IRSEC, pp. 165–172. http://dx.doi.org/10.1109/IRSEC.2016.7984021.

Tavakoli, A., Forouzanfar, M., 2020a. A self-constructing Lyapunov neural network controller to track global maximum power point in PV systems. Int. Trans. Electr. Energy Syst. 30 (6), 12391.

Tavakoli, A., Forouzanfar, M., 2020b. A self-constructing Lyapunov neural network controller to track global maximum power point in PV systems. Int. Trans. Electr. Energy Syst. 30, e12391. http://dx.doi.org/10.1002/2050-7038.12391.

Yilmaz, U., Turksoy, O., Teke, A., 2019. Improved MPPT method to increase accuracy and speed in photovoltaic systems under variable atmospheric conditions. Int. J. Electr. Power Energy Syst. 113, 634–651.